



Linnartz, J. F., Müller, C. S. A., Hsu, Y-T., Hussey, N. E., Carrington, A., Breth Nielsen, C., Wiedmann, S., & et, A. (2022). Fermi surface and nested magnetic breakdown in WTe₂. *Physical Review Research*, 4(1), [L012005]. <https://doi.org/10.1103/PhysRevResearch.4.L012005>

Publisher's PDF, also known as Version of record

License (if available):
CC BY

Link to published version (if available):
[10.1103/PhysRevResearch.4.L012005](https://doi.org/10.1103/PhysRevResearch.4.L012005)

[Link to publication record in Explore Bristol Research](#)
PDF-document




This is the final published version of the article (version of record). It first appeared online via American Physical Society at <https://doi.org/10.1103/PhysRevResearch.4.L012005>. Please refer to any applicable terms of use of the publisher.

University of Bristol - Explore Bristol Research

General rights

This document is made available in accordance with publisher policies. Please cite only the published version using the reference above. Full terms of use are available: <http://www.bristol.ac.uk/red/research-policy/pure/user-guides/ebr-terms/>

Fermi surface and nested magnetic breakdown in WTe₂

J. F. Linnartz,^{1,2} C. S. A. Müller,^{1,2} Yu-Te Hsu,^{1,2} C. Breth Nielsen ³ M. Bremholm,³
N. E. Hussey ^{1,2,4} A. Carrington,^{4,*} and S. Wiedmann ^{1,2,†}

¹High Field Magnet Laboratory (HFML-EMFL), Radboud University, Toernooiveld 7, Nijmegen 6525 ED, Netherlands

²Radboud University, Institute for Molecules and Materials, Nijmegen 6525 AJ, Netherlands

³Department of Chemistry and iNANO, Aarhus University, Langelandsgade 140, DK-8000 Aarhus C, Denmark

⁴H.H. Wills Physics Laboratory, University of Bristol, Tyndall Avenue, BS8 1TL, United Kingdom



(Received 21 July 2021; revised 29 October 2021; accepted 6 December 2021; published 18 January 2022)

We report a detailed Shubnikov-de Haas (SdH) study on the Weyl type-II semimetal WTe₂ in magnetic fields up to 29 T. By using the SdH results to guide our density functional theory calculations, we are able to accurately determine its Fermi surface by employing a moderate Hubbard U term, which is an essential step in explaining the unusual electronic properties of this much studied material. In addition to the fundamental orbits, we observe magnetic breakdown, which can consistently be explained within the model of a Russian-doll nested Fermi surface of electron and hole pockets. The onset of magnetic breakdown in WTe₂ is solely determined by impurity damping in contrast to magnetic breakdown scenarios in other metallic systems.

DOI: [10.1103/PhysRevResearch.4.L012005](https://doi.org/10.1103/PhysRevResearch.4.L012005)

The layered transition-metal dichalcogenide WTe₂ provides a versatile platform to investigate topologically nontrivial phases [1]. Bulk WTe₂ in the T_d phase has been identified as the prototypical example of a Weyl type-II semimetal [2,3]. In the past few years, particular attention has been paid to the observation of a large, quadratic, and nonsaturating magnetoresistance (MR) up to 60 T, a signature of a perfectly compensated semimetal [4]. Bound by van der Waals interaction, two-dimensional (2D) layers of WTe₂ can also be exfoliated down to a monolayer. Through conventional gating techniques, various phases of matter such as the quantum spin Hall effect [5], superconductivity in a monolayer [6], and room-temperature vertical ferroelectricity in its bi- and trilayer form [7] have been observed.

The Fermi surface (FS) of bulk WTe₂ has been investigated through angle-resolved photoemission spectroscopy (ARPES) [8–15] and quantum oscillation (QO) experiments [10,14,16–22]. With previous density functional theory (DFT) band-structure calculations, however, it has proved challenging to correctly explain the size and shape of the small Fermi pockets [4,8–10,12,13,15–19,22].

The material has two mirror symmetries and consequently, there are two groups of electron and hole pockets, see Fig. 2(d). The majority of experimental investigations conclude that the FS does indeed comprise two pairs of electronlike pockets and two pairs of holelike pockets, the latter located near the center of the Brillouin zone, sandwiched

between the two pairs of electron pockets. Due to the lack of inversion symmetry in WTe₂, the spin-orbit interaction leads to a Dresselhaus spin splitting of the bands and hence the electron and hole FS consist of nested Russian-doll pairs [16,22]. A question remains, however, regarding the exact location of the Fermi level and whether the hole pockets are connected over the Γ point forming a dog-bone-shaped hole orbit [9,19] or if additional electron pockets reside in the vicinity of the Γ point [14].

One way to solve this longstanding puzzle is to exploit the phenomenon of magnetic breakdown (MB), i.e., tunneling of quasiparticles between distinct (adjacent) pockets of the FS above a threshold magnetic field. This leads to the formation of new orbits consisting of linear combinations of the fundamental frequencies of the associated pockets and thereby constraining further the topology of the FS. Indeed, previous QO studies have shown that MB might occur in WTe₂ [16–18,21], though a robust identification of these orbits has not yet been done. Additionally, O'Brien *et al.* proposed that magnetic breakdown in WTe₂ occurs between one electron and one hole pocket due to the specific cone structure of a Weyl type-II semimetal whereby electron and hole bands touch each other in k space [23]. Knowing whether this scenario is actually manifested in WTe₂ depends on a detailed knowledge of the Fermi surface, which is currently lacking.

In this Letter, we present high-field magnetotransport experiments on a mm-sized WTe₂ sample down to ³He temperatures. Our analysis of the observed Shubnikov-de Haas (SdH) oscillations, when combined with our DFT calculations determines the precise electronic structure of WTe₂ close to the Fermi level. Our subsequent analysis confirms the nested Russian-doll arrangement but suggests that MB can only occur between pockets of the same sign. Moreover, and in contrast with other metallic systems, the onset of MB is found to be solely determined by impurity damping.

*a.carrington@bristol.ac.uk

†steffen.wiedmann@ru.nl

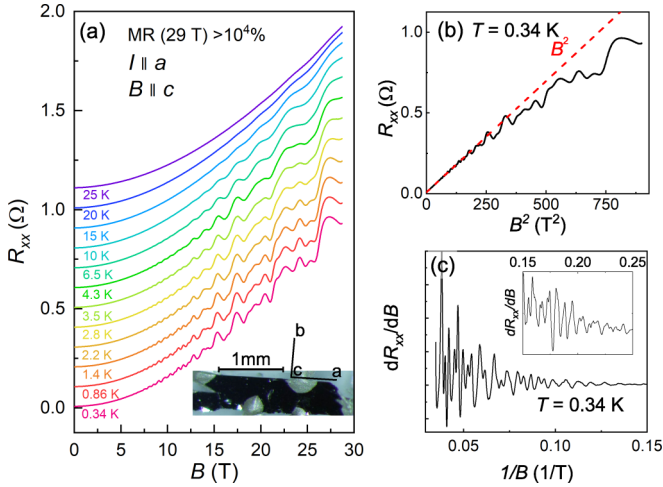


FIG. 1. (a) Resistance R_{xx} as a function of magnetic field measured for various temperatures up to 25 K. The curves are offset vertically for clarity. The inset shows the mm-sized exfoliated sample. (b) R_{xx} plotted versus B^2 to highlight the quadratic behavior of the MR. (c) dR_{xx}/dB as a function of $1/B$ at 0.34 K. The inset shows the low-field part of $dR_{xx}/dB(1/B)$.

WTe₂ flakes were grown by vapor transport method using iodine as the transport agent. Tungsten (99.9%) and tellurium (99.9999%) powders were ground together, pressed into a pellet and prereacted in an evacuated silica tube at 750 °C for two days. The product was then reground, pressed into a pellet again and loaded into a silica tube with iodine pieces. The tube was placed off center in a tube furnace to create a temperature gradient of 50 °C between 850 and 800 °C and left to grow for two weeks. Figure 1(a) shows the longitudinal resistance R_{xx} for the sample under study (residual resistance ratio RRR = 30) for various temperatures with the magnetic field B applied along the c axis while the current is passed along the a axis of the sample. For all temperatures, QOs are superimposed on a B^2 MR of $\sim 12000\%$ at maximum field. The quadratic MR persists up to 15 T indicating perfect charge carrier compensation before crossing over to a $B^{1.7}$ dependence up to the maximum field, see Fig. 1(b). In Fig. 1(c), dR_{xx}/dB is plotted as a function of $1/B$ in order to highlight the emergence of QOs for $B > 4$ T at $T = 0.34$ K.

In Fig. 2(a), fast Fourier transforms (FFTs) of the dR_{xx}/dB data of Fig. 1(c) are presented for different magnetic field ranges. For the lowest field range [4–10] T, four distinct peaks are observed, which we mark as α , β , γ , and δ following the labeling of Ref. [16]. For details, we refer to Fig. S1 in the Supplemental Material [25]. Using the Onsager relation, we relate the frequencies f observed in the FFT spectrum to the extremal areas A_f of the individual pockets: $f = (\hbar/2\pi e)A_f$ [26]. Above a threshold magnetic field ($B \geq 8$ T), the QO pattern becomes more complex. In addition to the well-developed low-frequency peaks, a high-frequency orbit at 240 T appears [see the [5–28.7 T] spectrum in Fig. 2(a)]. This frequency corresponds approximately to the sum of the individual frequencies of the α and δ orbits, $f_{\alpha+\delta} = f_{\alpha} + f_{\delta}$ and is thus a viable signature of MB that will be discussed later.

The angle dependence of the SdH oscillations is presented in Fig. 2(b). B_{\perp} can be determined by maximizing R_{xx} due to

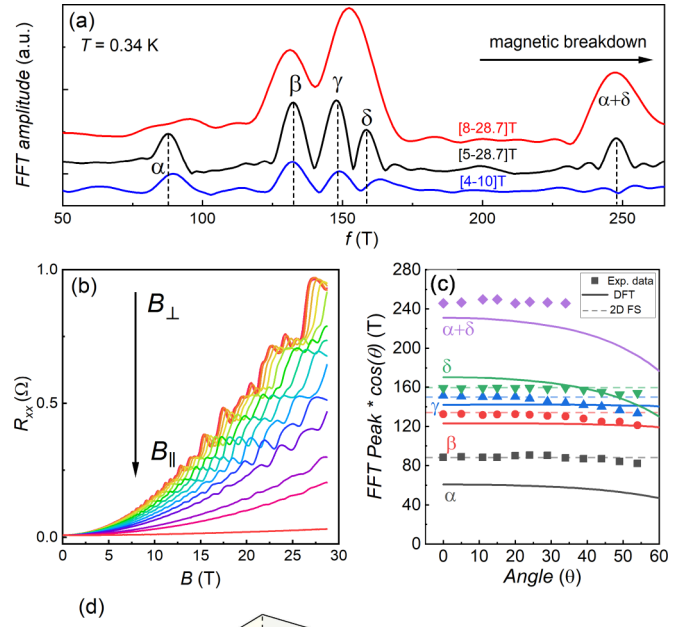


FIG. 2. (a) FFT spectrum (Hann window) of the SdH signal for various magnetic field ranges. At low B , the individual pockets of the FS are observed. The orbits are labeled with greek letters. With increasing field range, MB occurs and an additional orbit with frequency $f_{\alpha+\delta}$ emerges. (b) R_{xx} for different tilt angles with 5° increments at $T = 1.4$ K. (c) Rotation from (001) to (010). Maxima of the FFT peaks as a function of tilt angle are indicated with solid symbols. The dashed lines correspond to the $1/\cos(\theta)$ dependence expected for a two-dimensional system, the solid lines to the DFT calculation. (d) Three-dimensional FS of WTe₂ obtained via LDA+U DFT calculation with $U = 3$ eV.

the sensitivity of the MR of WTe₂ to changes in tilt angle [27]. A commercial Hall probe has been used to extract precise values for the other tilt angles. Both the MR and the QO amplitudes strongly decrease as the sample is rotated from B_{\perp} (i.e., B parallel to the c axis) to B_{\parallel} (B parallel to the a axis). In order to map the FS of WTe₂, the frequencies of peaks obtained from the FFT spectrum [5–28.7 T] multiplied by $\cos \theta$ are plotted as a function of tilt angle θ in Fig. 2(c) to better visualize the quasi-2D nature of the pockets. With increasing θ , the QO amplitudes of the individual orbits become more and more damped and eventually vanish above 55°. The MB orbit, $f_{\alpha+\delta}$ can be observed up to $\theta = 30^\circ$, as reported previously [16]. The persistence of this orbit over such a wide angular range contrasts markedly with recent observations of MB in nodal-line semimetals [28–30] where the MB orbits are found to vanish exponentially with increasing tilt angles.

To determine the Fermi surface from our extremal orbit size and mass data we use GGA+U DFT calculations [31,32]

TABLE I. Identified orbits, extracted frequencies and cyclotron masses from the experiment in the range from [5–28.7 T] compared to the frequencies and cyclotron masses from the DFT calculations.

Orbit	Type	f (T)	m_c (m_e)	f_{DFT} (T)	$m_{c,DFT}$ (m_e)
α	h	88	0.47 ± 0.06	66	0.43
β	e	133	0.40 ± 0.02	134	0.38
γ	e	148	0.40 ± 0.03	155	0.35
δ	h	158	0.46 ± 0.04	186	0.58

with an experimentally determined structure [33]. The calculated Fermi surface is shown in Fig. 2(d) and Fig. 4(e) and consists of two pairs of hole pockets and two pairs of electron pockets, which are symmetry distinct. Each pair of electron and hole pockets is nested within each other and the surfaces are symmetrically reflected in the Γ - Z - Y plane. From this Fermi surface we identify the α and δ orbits as originating from the two hole pockets, and β and δ from the two electron pockets. Each FS pocket is found to have a single extremal orbit. For such small FS volumes, small shifts in the band energies are often needed to get perfect agreement with experiment. However, for WTe_2 , we find that in addition a moderate $U \simeq 3$ eV must also be employed for the tungsten d orbitals in order to explain the observed value of m_c for the hole pockets. Without this, the calculated mass is a factor ~ 2 too high, even after shifting the band energies to match the observed frequencies. Physically, U models the on-site Coulomb repulsion; an approach which has also been employed, for example, for the related material MoTe_2 where a similar Hubbard U value was found [34,35]. Although the agreement with experiment is not perfect, the residual differences [see Table I and Fig. 2(c)] are acceptably small. Further details of the calculations, including how the results depend on U , are shown in the Supplemental Material [25].

Extraction of the cyclotron masses, m_c , of the individual pockets of the FS has proven to be a challenge for the β , γ , and δ peaks as they are separated by only $\simeq 10$ T in the FFT spectrum, and a proper range has to be chosen to avoid convolution of their FFT peaks. In Fig. 3(a), the range [5–28.7 T] of the FFT spectrum, taken from dR_{xx}/dB , is plotted for different temperatures up to 10 K. Figures 3(b), 3(d), 3(e), 3(f) display the FFT amplitudes of the individual peaks as a function of temperature fitted to the temperature-dependent term of the Lifshitz-Kosevich formula, $R_T = X/\sinh[X]$ with $X = \frac{2\pi^2 k_B m_c^* T}{\hbar e \langle B \rangle}$, where $\langle 1/B \rangle = \frac{(1/B_{\min}) + (1/B_{\max})}{2}$. Additional details concerning the mass extraction are discussed in the Supplemental Material [25]. The experimentally extracted cyclotron masses m_c and those obtained from DFT calculations for each individual pocket are summarized in Table I. In order to separate the FFT peaks a relatively large field range [5–28.7 T] is needed, which could in principle lead to an underestimate of the masses. However, the variation in m_c for the α pocket on the field range shown in Fig. 3(c), along with additional analysis presented in the Supplemental Material [25] shows this effect is within our errors here.

A further constraint of the FS topology can be made by analyzing the MB orbits. Magnetic breakdown occurs if the applied magnetic field $B > B_0 \approx (\hbar/e)(k_g/2)^2$, where k_g is the breakdown gap in k space. From our DFT calculations, we

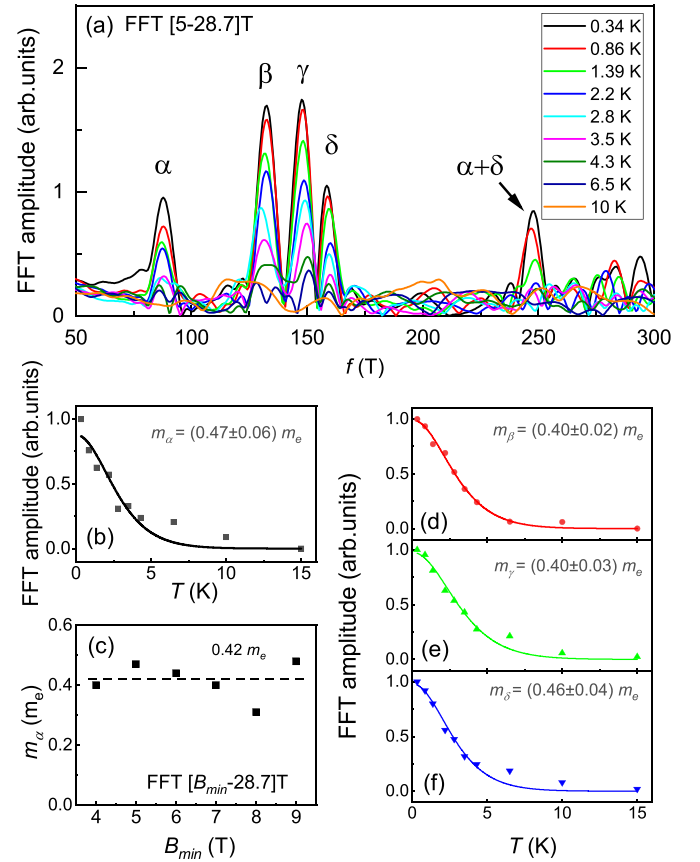


FIG. 3. (a) FFT spectra in the field range [5–28.7 T] for different temperatures up to 10 K for $B \parallel c$. (b) Extraction of m_c for the α pocket and (c) its corresponding range analysis in different field ranges by varying B_{\min} . (d)–(f) Extraction of m_c for the other individual pockets β , γ , and δ of the FS.

extract a gap of $B_0 = 0.2$ T for electrons and 0.5 T for holes, respectively. This implies that the Dingle field is around one order of magnitude larger than B_0 , see Supplemental Material [25]. Therefore, MB is determined by impurity damping in WTe_2 . In Fig. 4(a), the FFT spectra obtained from dR_{xx}/dB containing all of the observed MR orbits are shown for several temperatures between 0.34 and 6.5 K in the field range [8–28.7 T]. In addition to the $\alpha + \delta$ orbit, we identify four more MB orbits: $\beta + \gamma$, $2\alpha + \delta$, $\alpha + 2\delta$, $3\alpha + \delta$. Given our experimental resolution, we are only able to extract the cyclotron masses of the $\alpha + \delta$, $\beta + \gamma$, and $2\alpha + \delta$ orbits, each of which corresponds to the sum of the masses of the individual pockets [24,26,28–30]. Their absolute values are summarized in Table II and the corresponding fits are presented in Figs. 4(b)–4(d) in which the R_T term has been fitted to the T -dependent FFT amplitudes.

The appropriateness of the MB scenario in WTe_2 including the extracted cyclotron masses of the breakdown orbits and the persistence of the $\alpha + \delta$ orbit to large tilt angles, is corroborated by our DFT calculations. Knowing the topology of the Fermi surface and having determined the masses of the breakdown orbits enables us now to elucidate the origin of MB in WTe_2 and thus the precise FS. The scenarios based on electron-hole MB [23] and the possibility of hole-hole

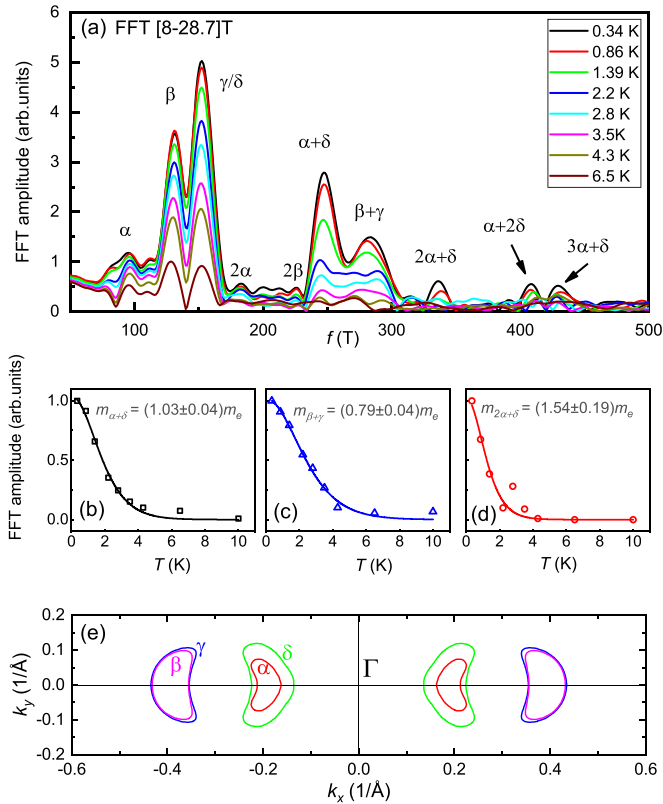


FIG. 4. (a) FFT spectrum for the field range [8–28.7 T] for different temperatures up to 6.5 K. The corresponding individual and breakdown orbits are labeled. (b)–(d) FFT amplitude as a function of T to extract m_c of the MB orbits with the frequencies $f_{\alpha+\delta}$, $f_{\beta+\gamma}$ and $f_{2\alpha+\delta}$. (e) Cut of the FS in the k_x - k_y plane highlighting the nested Russian-doll configuration.

tunneling across the Γ point [16] can be excluded due to the observed breakdown frequencies and (large) finite gaps in momentum space, see Fig. 4(e), making quasiparticle tunneling within our magnetic field range impossible. Another key observation is the absence of the 2δ pocket in our FFT spectra. If tunneling occurred over the Γ point, QOs with a frequency $f_{2\delta}$ would be easily observed in the FFT spectra.

In light of these considerations, the most likely scenario that is consistent with all our experimental findings is the one in which magnetic breakdown occurs between Russian-doll nested electron or hole pockets in WTe_2 . This scenario, supported by our DFT calculations allows for either electron-

TABLE II. Magnetic breakdown orbits and their extracted cyclotron masses using the field fitting range [8–28.7 T].

Orbit	f (T)	m_c (m_e)	type
$\alpha + \delta$	247	1.03 ± 0.04	hole-hole
$\beta + \gamma$	283	0.79 ± 0.04	electron-electron
$2\alpha + \delta$	336	1.54 ± 0.19	hole-hole

electron ($\beta + \gamma$) or hole-hole ($\alpha + \delta$) tunneling, see Fig. S7 [25], within the nested pockets giving rise to frequencies of the MB orbits that we observe in the FFT spectra. The α pocket is situated inside the δ pocket with a similar curvature along one direction k space [see Fig. 4(e)] enabling quasiparticles undergo magnetic breakdown. This scenario explains why this orbit survives out to large tilt angles as the tunneling gap will not markedly change with increasing θ .

In conclusion, we have performed magnetotransport experiments up to 29 T combined with DFT calculations that enable us to precisely determine the Fermi surface of WTe_2 . Four individual pockets and their corresponding cyclotron masses have been identified and extracted. The Fermi surface exhibits quasi-2D behavior upon tilting the magnetic field away from the c axis of the crystal. All observed orbits originating from magnetic breakdown have been assigned that further constrains the topology of the Fermi surface. The unprecedented resolution of our high-field study enables us to extract the cyclotron masses of MB orbits and together with the longevity of one of the MB orbits at finite tilt angles, allows for an unambiguous determination of magnetic breakdown in WTe_2 that is seen to occur between two electron and hole pockets in a nested Russian-doll configuration.

This work was supported by HFML-RU/NWO-I, a member of the European Magnetic Field Laboratory (EMFL) and by the UK Engineering and Physical Sciences Research Council (Grant No. EP/R011141/1). This publication is part of the project TOPCORE (OCENW.GROOT.2019.048) of the research program NWO – GROOT which is financed by the Dutch Research Council (NWO). We gratefully acknowledge funding from the VILLUM FOUNDATION via the Centre of Excellence for Dirac Materials (11744). M.B. acknowledges the Danish Council for Independent Research, Natural Sciences under the Sapere Aude program (Grant No. 7027-00077B). We thank Malte Rösner and Kamran Behnia for helpful discussions.

- [1] X.-C. Pan, X. Wang, F. Song, and B. Wang, The study on quantum material WTe_2 , *Adv. Phys.* **X 3**, 1468279 (2018).
- [2] A. Soluyanov, D. Gresch, Z. Wang, Q. S. Wu, M. Troyer, X. Dai, and B. A. Bernevig, Type-II Weyl semimetals, *Nature (London)* **527**, 495 (2015).
- [3] N. P. Armitage, E. J. Mele, and A. Vishwanath, Weyl and Dirac semimetals in three-dimensional solids, *Rev. Mod. Phys.* **90**, 015001 (2018).
- [4] M. Ali, J. Xiong, S. Flynn, J. Tao, Q. D. Gibson, L. M. Schoop, T. Liang, N. Haldolaarachchige, M. Hirschberger, N. P. Ong, and R. J. Cava, Large, non-saturating magnetoresistance in WTe_2 , *Nature (London)* **514**, 205 (2014).
- [5] S. Wu, V. Fatemi, Q. D. Gibson, K. Watanabe, T. Taniguchi, R. J. Cava, and P. Jarillo-Herrero, Observation of the quantum spin Hall effect up to 100 Kelvin in a monolayer crystal, *Science* **359**, 76 (2018).
- [6] E. Sajadi, T. Palomaki, Z. Fei, W. Zhao, P. Bement, C. Olsen, S. A. Luescher, X. Xu, J. A. Folk, and D. H. Cobden, Gate-induced superconductivity in a monolayer topological insulator, *Science* **362**, 922 (2018).
- [7] Z. Fei, W. Zhao, T. A. Palomaki, B. Sun, M. K. Miller, Z. Zhao, J. Yan, X. Xu, and D. H. Cobden, Ferroelectric switching of a two-dimensional metal, *Nature (London)* **560**, 336 (2018).

- [8] I. Pletikosić, M. N. Ali, A. V. Fedorov, R. J. Cava, and T. Valla, Electronic Structure Basis for the Extraordinary Magnetoresistance in WTe_2 , *Phys. Rev. Lett.* **113**, 216601 (2014).
- [9] J. Jiang, F. Tang, X. C. Pan, H. M. Liu, X. H. Niu, Y. X. Wang, D. F. Xu, H. F. Yang, B. P. Xie, F. Q. Song, P. Dudin, T. K. Kim, M. Hoesch, P. K. Das, I. Vobornik, X. G. Wan, and D. L. Feng, Signature of Strong Spin-Orbital Coupling in the Large Nonsaturating Magnetoresistance Material WTe_2 , *Phys. Rev. Lett.* **115**, 166601 (2015).
- [10] Y. Wu, N. H. Jo, M. Ochi, L. Huang, D. Mou, S. L. Bud'ko, P. C. Canfield, N. Trivedi, R. Arita, and A. Kaminski, Temperature-Induced Lifshitz Transition in WTe_2 , *Phys. Rev. Lett.* **115**, 166602 (2015).
- [11] Y. Wu, D. Mou, N. H. Jo, K. Sun, L. Huang, S. L. Bud'ko, P. C. Canfield, and A. Kaminski, Observation of Fermi arcs in the type-II Weyl semimetal candidate WTe_2 , *Phys. Rev. B* **94**, 121113(R) (2016).
- [12] C. Wang, Y. Zhang, J. Huang, S. Nie, G. Liu, A. Liang, Y. Zhang, B. Shen, J. Liu, C. Hu, Y. Ding, D. Liu, Y. Hu, S. He, L. Zhao, L. Yu, J. Hu, J. Wei, Z. Mao, Y. Shi *et al.*, Observation of Fermi arc and its connection with bulk states in the candidate type-II Weyl semimetal WTe_2 , *Phys. Rev. B* **94**, 241119(R) (2016).
- [13] D. Di Sante, P. K. Das, C. Bigi, Z. Ergönenc, N. Gürtler, J. A. Krieger, T. Schmitt, M. N. Ali, G. Rossi, R. Thomale, C. Franchini, S. Picozzi, J. Fujii, V. N. Strocov, G. Sangiovanni, I. Vobornik, R. J. Cava, and G. Panaccione, Three-Dimensional Electronic Structure of the Type-II Weyl Semimetal WTe_2 , *Phys. Rev. Lett.* **119**, 026403 (2017).
- [14] Y. Wu, N. H. Jo, D. Mou, L. Huang, S. L. Bud'ko, P. C. Canfield, and A. Kaminski, Three-dimensionality of the bulk electronic structure in WTe_2 , *Phys. Rev. B* **95**, 195138 (2017).
- [15] P. K. Das, D. Di Sante, F. Cilento, C. Bigi, D. Kopic, D. Soranzio, A. Sterzi, J. A. Krieger, I. Vobornik, J. Fujii, T. Okuda, V. N. Strocov, M. B. H. Breese, F. Parmigiani, G. Rossi, S. Picozzi, R. Thomale, G. Sangiovanni, R. J. Cava, and G. Panaccione, Electronic properties of candidate type-II Weyl semimetal WTe_2 . A review perspective, *Electron. Struct.* **1**, 014003 (2019).
- [16] Z. Zhu, X. Lin, J. Liu, B. Fauqué, Q. Tao, C. Yang, Y. Shi, and K. Behnia, Quantum Oscillations, Thermoelectric Coefficients, and the Fermi Surface of Semimetallic WTe_2 , *Phys. Rev. Lett.* **114**, 176601 (2015).
- [17] P. L. Cai, J. Hu, L. P. He, J. Pan, X. C. Hong, Z. Zhang, J. Zhang, J. Wei, Z. Q. Mao, and S. Y. Li, Drastic Pressure Effect on the Extremely Large Magnetoresistance in WTe_2 : Quantum Oscillation Study, *Phys. Rev. Lett.* **115**, 057202 (2015).
- [18] D. Rhodes, S. Das, Q. R. Zhang, B. Zeng, N. R. Pradhan, N. Kikugawa, E. Manousakis, and L. Balicas, Role of spin-orbit coupling and evolution of the electronic structure of WTe_2 under an external magnetic field, *Phys. Rev. B* **92**, 125152 (2015).
- [19] X. C. Pan, Xu. Chen, H. Liu, Y. Feng, Z. Wei, Y. Zhou, Z. Chi, L. Pi, F. Yen, F. Song, X. Wan, Z. Yang, B. Wang, G. Wang, and Y. Zhang, Pressure-driven dome-shaped superconductivity and electronic structural evolution in tungsten ditelluride, *Nat. Commun.* **6**, 7805 (2015).
- [20] K. G. Rana, F. K. Dejene, N. Kumar, C. R. Rajamathi, K. Sklarek, C. Felser, and S. S. P. Parkin, Thermopower and unconventional nernst effect in the predicted Type-II weyl semimetal WTe_2 , *Nano Lett.* **18**, 6591 (2018).
- [21] S. Onishi, R. Jha, A. Miyake, R. Higashinaka, T. D. Matsuda, M. Tokunaga, and Y. Aoki, Deviation from the Kohler's rule and Shubnikov-de Haas oscillations in type-II Weyl semimetal WTe_2 : High magnetic field study up to 56 T, *AIP Adv.* **8**, 101330 (2018).
- [22] N. H. Jo, L.-L. Wang, P. P. Orth, S. L. Bud'ko, and P. C. Canfield, Magnetoelastoresistance in WTe_2 : Exploring electronic structure and extremely large magnetoresistance under strain, *Proc. Natl. Acad. Sci. USA* **116**, 25524 (2019).
- [23] T. E. O'Brien, M. Diez, and C. W. J. Beenakker, Magnetic Breakdown and Klein Tunneling in a Type-II Weyl Semimetal, *Phys. Rev. Lett.* **116**, 236401 (2016).
- [24] M. I. Kaganov, and A. A. Slutskin, Coherent magnetic breakdown, *Phys. Rep.* **98**, 189 (1983).
- [25] See Supplemental Material at <http://link.aps.org/supplemental/10.1103/PhysRevResearch.4.L012005> for details on the assignment of individual pockets of the Fermi surface, DFT band-structure calculations, mass determination, and magnetic breakdown in the nested Russian-doll configuration.
- [26] D. Shoenberg, *Magnetic Oscillations in Metals* (Cambridge University Press, Cambridge, 1984).
- [27] L. R. Thoutam, Y. L. Wang, Z. L. Xiao, S. Das, A. Luican-Mayer, R. Divan, G. W. Crabtree, and W. K. Kwok, Temperature-Dependent Three-Dimensional Anisotropy of the Magnetoresistance in WTe_2 , *Phys. Rev. Lett.* **115**, 046602 (2015).
- [28] S. Pezzini, M. R. van Delft, L. M. Schoop, B. V. Lotsch, A. Carrington, M. I. Katsnelson, N. E. Hussey, and S. Wiedmann, Unconventional mass enhancement around the Dirac nodal loop in ZrSiS , *Nat. Phys.* **14**, 178 (2018).
- [29] M. R. van Delft, S. Pezzini, T. Khouri, C. S. A. Müller, M. Breitreiz, L. M. Schoop, A. Carrington, N. E. Hussey, and S. Wiedmann, Electron-Hole Tunneling Revealed by Quantum Oscillations in the Nodal-Line Semimetal HfSiS , *Phys. Rev. Lett.* **121**, 256602 (2018).
- [30] C. S. A. Müller, T. Khouri, M. R. van Delft, S. Pezzini, Y.-T. Hsu, J. Ayres, M. Breitreiz, L. M. Schoop, A. Carrington, N. E. Hussey, and S. Wiedmann, Determination of the Fermi surface and field-induced quasiparticle tunneling around the Dirac nodal loop in ZrSiS , *Phys. Rev. Research* **2**, 023217 (2020).
- [31] P. Blaha, K. Schwarz, G. K. H. Madsen, D. Kvasnicka, and J. Luitz, WIEN2k (Karlheinz Schwarz, Techn. Universität Wien, Austria, 2001).
- [32] J. P. Perdew, K. Burke, and M. Ernzerhof, Generalized Gradient Approximation Made Simple, *Phys. Rev. Lett.* **77**, 3865 (1996).
- [33] A. Mar, S. Jobic, and J. A. Ibers, Metal-metal vs tellurium-tellurium bonding in WTe_2 and its ternary variants TaIrTe_4 and NbIrTe_4 , *J. Am. Chem. Soc.* **114**, 8963 (1992).
- [34] N. Aryal and E. Manousakis, Imporance of electron correlations in understanding photoelectron spectroscopy and Weyl character of MoTe_2 , *Phys. Rev. B* **99**, 035123 (2019).
- [35] Y. J. Hu, W. C. Yu, K. To Lai, D. Sun, F. F. Balakirev, W. Zhang, J. Y. Xie, K. Y. Yip, E. I. Paredes Aulestia, R. Jha, R. Higashinaka, T. D. Matsuda, Y. Yanase, Y. Aoki, and S. K. Goh, Detection of Hole Pockets in the Candidate Type-II Weyl Semimetal MoTe_2 from Shubnikov-de Haas Quantum Oscillations, *Phys. Rev. Lett.* **124**, 076402 (2020).